



Thermodynamic model and Raman spectra of MgO–P₂O₅ glasses

Branislav Hruška¹ · Rajesh Dagupati¹ · Mária Chromčíková^{2,3} · Aleksandra Nowicka¹ · Jan Macháček⁴ · Marek Liška^{2,3} · Francisco Munoz⁵

Received: 14 January 2020 / Accepted: 3 July 2020
© Akadémiai Kiadó, Budapest, Hungary 2020

Abstract

The structure of binary glasses $x\text{MgO}\cdot(1-x)\text{P}_2\text{O}_5$ ($x=0.30, 0.35, 0.40, 0.45, 0.50,$ and 0.55) was studied by thermodynamic model (TDM) of Shakhmatkin and Vedishcheva (SV) and Raman spectroscopy. In the TDM, six following system components were considered: MgO (M), P₂O₅ (P), MgO·2P₂O₅ (MP2), MgO·P₂O₅ (MP), 2MgO·P₂O₅ (M2P), 3MgO·P₂O₅ (M3P). The principal component analysis (PCA) of experimental Raman spectra resulted in three independent components. The baseline subtracted and thermally corrected Raman spectra were analyzed by the multivariate curve analysis (MCR) for three components. The MCR resulted in the Raman spectra and relative abundance of each component. The experimental spectra were reproduced by the MCR on the level of 99.9%. Correlation analysis attributed the MCR components to M2P, MP, and MP2. Then the Malfait's decomposition was performed based on the TDM-SV equilibrium molar amounts of system components (MP2, MP, and M2P) resulting in partial Raman spectra (PRS). Normalized MCR loadings coincide with normalized PRS. Adjusted scores were reproduced with good accuracy equilibrium molar amounts of system components.

Keywords Phosphate glass · MgO–P₂O₅ · Raman · TD model · Multivariate curve resolution

Introduction

When compared with silicate or borate glasses, phosphate glasses possess valuable properties, such as high refractive index, low melting temperature, and low absorption in the ultraviolet spectral range [1, 2]. On the other hand, phosphate glasses are characteristic by low chemical durability caused by the hygroscopicity of phosphorus pentoxide. The chemical stability and supplementary properties can be improved by adding different oxides of different valence to

the parent phosphate network [3, 4]. This large variability in composition makes phosphate glasses excellent candidates for various applications, namely in the field of metals sealing, photonics, medical and health care, vitrification of radioactive waste, etc. [5–11].

TDM-SV can be used to interpret the composition–structure–property relationships for a variety of multi-component glass-forming systems [12–19]. On the other hand, the model has to be checked by the comparison of its results with the structural data for various glasses and melts [17–21]. In our previous work [20, 22–24] we showed that the statistical analysis of the Raman spectra validated the TDM-SV for the Na₂O–B₂O₃, CaO–P₂O₅, and ZnO–P₂O₅ binary glass systems. The main aim of this work is to confirm the validity of the model by the analysis of Raman spectra of compositional series of Mg–P₂O₅ binary glasses.

Method

TDM-SV

In previous time, TDM-SV was successfully applied to the study of silicate glasses [12–20]. In this model oxide glasses

✉ Branislav Hruška
branislav.hruska@tuni.sk

¹ FunGlass, Alexander Dubček University of Trenčín, Študentská 2, Trenčín 911 50, Slovakia

² VILA – Joined Glass Centre of the IIC SAS, TnUAD, FChPT STU, Študentská 2, Trenčín 911 50, Slovakia

³ Institute of Inorganic Chemistry of Slovak Academy of Sciences, Dúbravská cesta 9, Bratislava 845 36, Slovakia

⁴ Faculty of Chemical Technology, University of Chemistry and Technology, Prague, Technická 5, Prague 166 28, Czech Republic

⁵ Institute of Ceramics and Glass (CSIC), Kelsen 5, 28049 Madrid, Spain

and melts are considered as the ideal equilibrium solutions consisting of products of chemical reactions between the oxides and from the un-reacted oxides. The stoichiometry of these products is given by the crystalline compounds found in the particular equilibrium phase diagram. Only the molar Gibbs energies of pure crystalline compounds, analytical composition of the system and temperature are used as input parameters. The equilibrium system composition is found by the minimization of the system's Gibbs energy with respect to the molar amount of each of the system's species [25]. The current thermodynamic databases containing molar Gibbs energy (such as FACT database [26, 27]) allow routine construction TDM-SV for many multi-component melts and glasses.

Malfait's decomposition of Raman spectra and MCR

Malfait et al. [28–30] proposed the method of numerical analysis of Raman spectra based on the knowledge of the system composition. The basic assumption is that the Raman spectra are the sum of partial Raman spectra of individual species multiplied by their molar amount. Raman spectra of a series of glasses form linear vector space with dimensionality given by the number of independent species (i.e. species with different PRS that independently change their concentration). Arbitrary scaling is supposed for each experimental spectrum, i.e. it is known with the exception of a multiplication factor. The number of independent components can be determined by the PCA [31, 32]. It is worth noting that in the field of thermal analysis the application of the PCA may be very advantageous [33]. The set of experimental Raman spectra is decomposed by the MCR method [34, 35] on the so-called loadings (i.e. spectra of quasi pure components) and so-called scores (i.e. relative abundances of these components). MCR method is frequently used in the field of spectroscopy, e.g. in connection with the FT IR spectra analysis [36]. It is important to emphasize that the knowledge of the system composition is not needed for the MCR analysis. The TDM-SV has to be validated by comparison of MCR results with the results of Malfait's spectra decomposition based on the results of TDM-SV.

Experimental

The glass batches were prepared from analytical grade ammonium dihydrogen phosphate ($\text{NH}_4\text{H}_2\text{PO}_4$) and barium carbonate (MgCO_3). Stoichiometric quantities of MgCO_3 and $\text{NH}_4\text{H}_2\text{PO}_4$ were placed into an alumina crucible after

being mixed in an agate mortar. In order to remove the water, ammonia, and carbon dioxide, the sample was slowly heated to 700 °C in an electrical furnace. Subsequently, the calcination products were melted at the temperature range of 1100–1200 °C, depending on their chemical composition. The resulting melt was poured onto a preheated (300 °C) brass mold and annealed for 2 h at the temperature that was approximately 5 °C under the glass transition temperature (T_g). The glass composition was checked by the RTG fluorescence spectroscopy (Bruker, Tiger S8). Small amounts of Al_2O_3 on the level of 1 mol % were found. This is a typical situation for melting of phosphate glasses in alumina crucibles [37].

The glass transition temperature was measured by thermo-mechanical analyzer TMA NETZSCH 402 with the vertical orientation of the measured sample. Prismatic glass samples with dimensions of approximately (5 × 5 × 20) mm were used. The cooling dilatometric curve was recorded at a cooling rate of 5 °C min⁻¹ in the temperature range below the glass softening temperature.

Raman spectra were obtained using Raman spectrometer (RENISHAW).

The 532 nm laser with the power of 28.5 mW was used with the spot of about 1 mm diameter. Baseline subtracted spectra were corrected by the Böse–Einstein population factor [38]:

$$I_{\text{cor}} = I_{\text{exp}} \nu_0^3 \frac{1 - \exp[-hc\nu/kT]}{(\nu_0 - \nu)^4} \quad (1)$$

where I_{exp} is the observed Raman intensity, I_{cor} is the corrected Raman intensity, ν_0 and ν are the wavenumber of the excitation laser and the Raman shift, T —the thermodynamic temperature, h —Planck constant, k —Boltzmann constant, and c —the speed of light.

Results and discussion

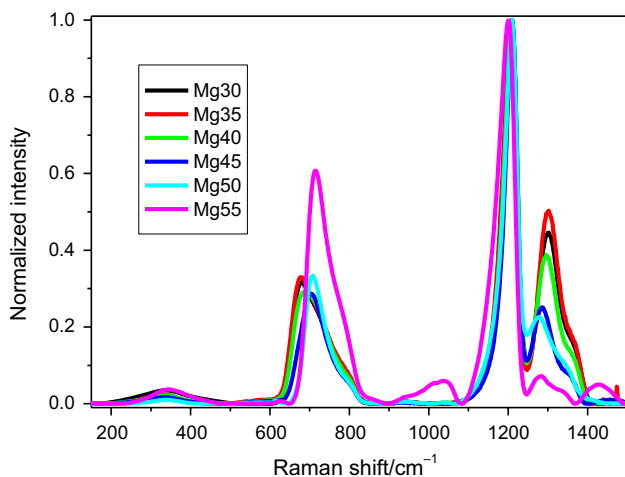
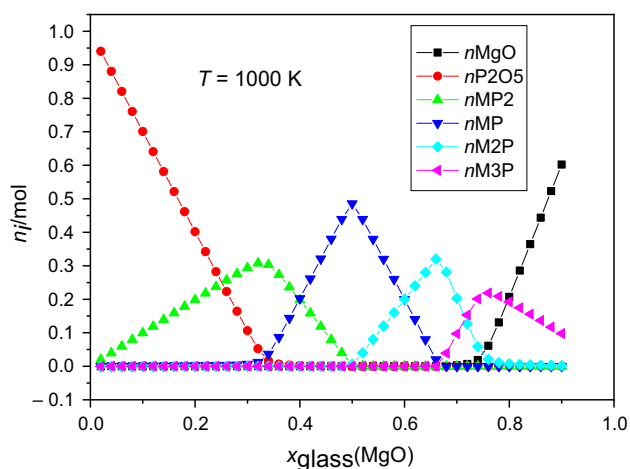
The measured

The measured values of the glass transition temperature, T_g , are summarized in Table 1. It can be seen that the glass transition temperature increases with the MgO content. Small irregularities can be probably attributed to the Al_2O_3 contamination.

Six normalized baseline subtracted and thermally corrected Raman spectra of $x\text{MgO} \cdot (1-x)\text{P}_2\text{O}_5$ ($x=0.30, 0.35, 0.40, 0.45, 0.50, 0.55$) glasses were analyzed (Fig. 1). The spectra were digitized with a wavenumber step of 2 cm⁻¹ between (150–1500) cm⁻¹. The baseline subtraction was

Table 1 Glass transition temperature, T_g , results of TDM-SV, and corresponding Q -distribution

x_{MgO}	$T_g \pm 2/\text{K}$	$n(\text{P})/\text{mol}$	$n(\text{MP2})/\text{mol}$	$n(\text{MP})/\text{mol}$	$n(\text{M2P})/\text{mol}$	$n(Q^3)/\text{mol}$	$n(Q^2)/\text{mol}$	$n(Q^1)/\text{mol}$
0.30	797	0.10	0.30	0.00	0.00	0.80	0.60	0.00
0.35	794	0.00	0.30	0.05	0.00	0.60	0.70	0.00
0.40	803	0.00	0.20	0.20	0.00	0.40	0.80	0.00
0.45	809	0.00	0.10	0.35	0.00	0.20	0.90	0.00
0.50	815	0.00	0.00	0.50	0.00	0.00	1.00	0.00
0.55	829	0.00	0.00	0.35	0.10	0.00	0.70	0.20


Fig. 1 Normalized and thermally corrected Raman spectra

Fig. 2 Thermodynamic model of Shakhmatkin and Vedishcheva—equilibrium molar amounts of system components at temperature $T=1000\text{ K}$

performed by the Renishaw software Wire ver. 4.2. It is worth noting that the baseline subtraction is not unique procedure and the result depends on various software user decisions.

The TDM-SV was evaluated well above T_g at the temperature of 1000 K (Fig. 2). Six system components, defined as the stable crystalline phases of the MgO–P₂O₅ phase diagram, were considered: MgO (M), P₂O₅ (P), MgO·2P₂O₅ (MP2), MgO·P₂O₅ (MP), 2MgO·P₂O₅ (M2P), 3MgO·P₂O₅ (M3P). The FACT database [26] was used to gather the Gibbs energies of the compounds listed above. The TDM behaves quasi-binary (i.e. maximum two system components can be found with nonzero abundance for each glass composition) even at temperature well above T_g . Therefore, the mass conservation law can be used to evaluate the equilibrium molar amounts of system components for all studied glass compositions at T_g . For the $x\text{MgO} \cdot (1-x)\text{P}_2\text{O}_5$ glass compositions we obtain the following relations:

- for $0 \leq x \leq 1/3$ only P and MP2 are present with a non-negligible equilibrium molar content, n_i .

$$n(\text{MP2}) = x \quad (2)$$

$$n(\text{P}) = 1 - 3x \quad (3)$$

- for $1/3 \leq x \leq 0.5$ only MP2 and MP are present with non-negligible equilibrium molar content:

$$n(\text{MP2}) = 1 - 2x \quad (4)$$

$$n(\text{MP}) = 3x - 1 \quad (5)$$

- for $0.5 \leq x \leq 2/3$ only MP and M2P are present with not negligible equilibrium molar content n_i .

$$n(\text{M2P}) = 2x - 1 \quad (6)$$

$$n(\text{MP}) = 2 - 3x \quad (7)$$

The resulting equilibrium molar amounts of system components and the corresponding Q -distributions are summarized in Table 1. Only three system components (i.e. M2P, MP, and MP2) and three Q -units (i.e. Q^3 , Q^2 , Q^1) are present in nonzero equilibrium molar amounts for all

studied glasses, with the exception of the $x_g(\text{MgO}) = 0.30$ glass, where a small amount of P_2O_5 was found.

MATLAB software [32] was used for the principle component analysis. The indicator function [31, 32] reached a minimum for three components and the Malinowski significance level falls below 5% for three components. The real error found for three components (0.009) was at the level of spectral noise. Thus PCA resulted in three independent components. Obtained result is in agreement with the result of TDM-SV.

The MCR [34, 35] performed for three components resulted in the relative abundances and Raman spectra of each component (Fig. 3). 99.9% of the spectral data variance was reproduced by the MCR method. Based on the high positive correlation between equilibrium molar amounts and scores, the loadings were assigned to the particular system components. This way, Loading 1 was attributed to M2P, Loading 2, to MP and Loading 3, to MP2.

The Malfait's spectral decomposition was performed with our own FORTRAN program JaneDove, using the equilibrium molar amounts of M2P, MP, and MP2. Such way partial Raman spectra (PRS) of M2P, MP, and MP2 were obtained. The experimental data were reproduced by the calculated spectra with a very good accuracy on the level of experimental noise (Fig. 4).

The normalized partial Raman spectra of M2P, MP, and MP2 are plotted in Fig. 3 where they are compared with the corresponding normalized MCR loadings. It can be seen that normalized MCR loadings are practically the same as the normalized PRS. The only exception is the non-physical negative part of PRS M2P ranging from 1215 to 1370 cm^{-1} caused probably by some singularity problems and small errors in baseline subtraction.

The MCR results are not unique. All experimental spectra and loadings (i.e. the spectra of "pure" component) can be scaled by multiplying or dividing them by an arbitrary positive constant. Such scaling of the

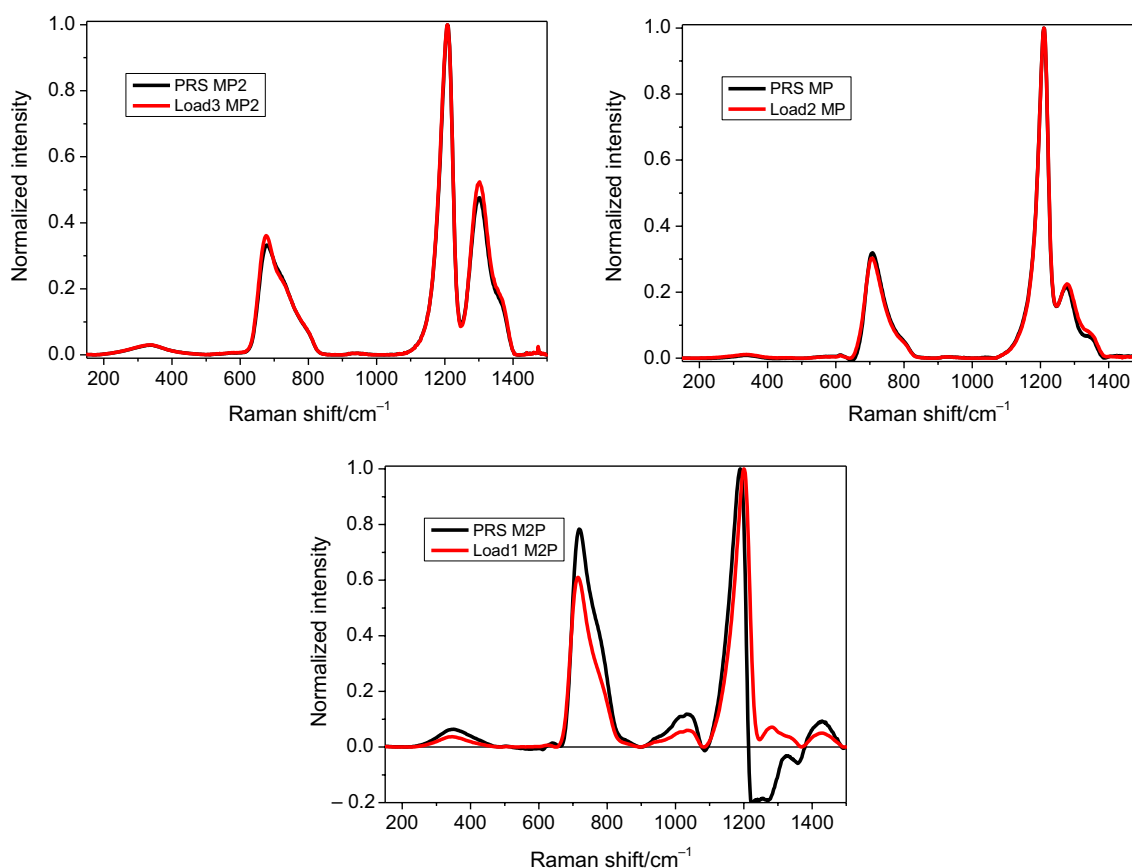


Fig. 3 Comparison of normalized partial Raman spectra MP2, MP, and M2P with corresponding normalized MCR loadings

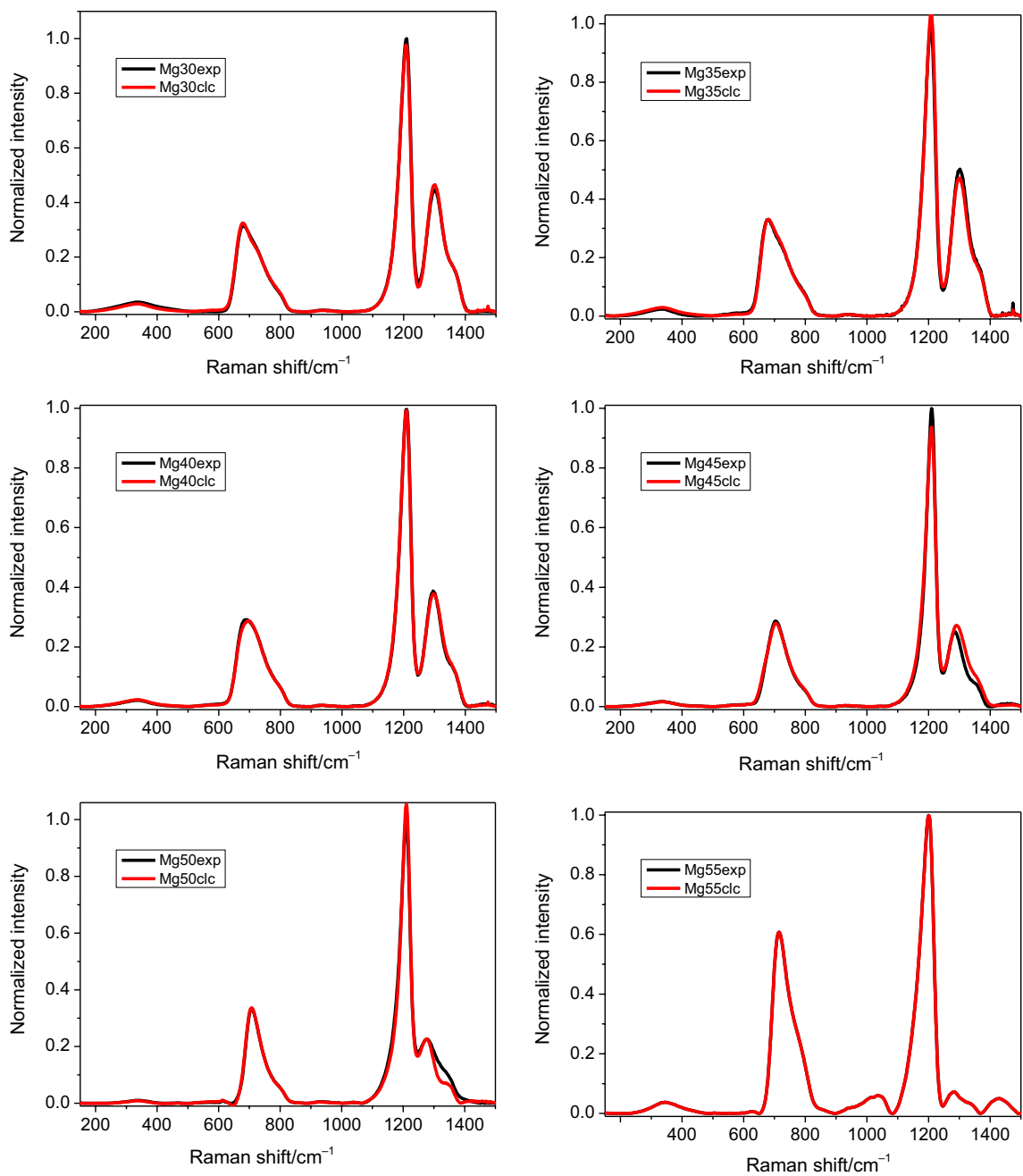


Fig. 4 Comparison of experimental and Malfait's method calculated Raman spectra

experimental spectra and loadings is reflected in the corresponding change of the scores. This way, scores can be adjusted to reproduce the equilibrium molar amounts of system components. Adjustment of the scores is done by minimizing the sum of the squares of the differences

between equilibrium molar amounts and corresponding scores. A good agreement between the adjusted scores and equilibrium molar amounts of system components is illustrated in Fig. 5.

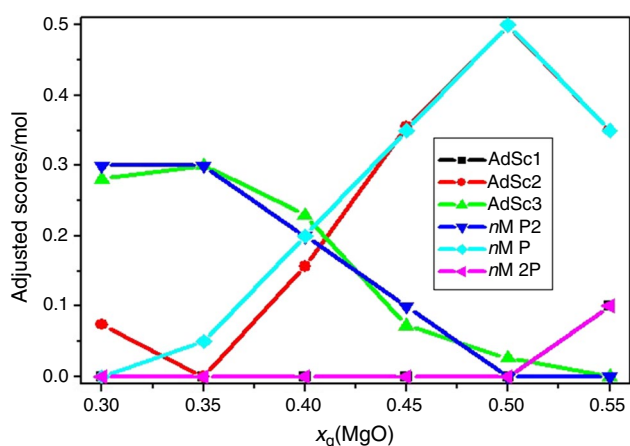


Fig. 5 Comparison of adjusted scores and equilibrium molar amounts of MP2, MP and M2P

Conclusions

The PRS obtained from the TDM-SV by the Malfait's method are in good agreement with the loadings obtained by the MCR method. MCR and Malfait's decomposition based on the results of TDM-SV reproduced the experimental spectra with good accuracy. The MCR loadings coincide with the Malfait's PRS and the adjusted scores agree well with the normalized molar amounts of system components. The obtained results confirm the TDM.

Acknowledgements This paper is created in the frame of the project FunGlass that has received funding from the European Union's Horizon 2020 research and innovation program under Grant Agreement No. 739566. This work was supported by The Slovak Grant Agency for Science under Grant VEGA 1/0064/18, and the project Centre for Functional and Surface Functionalized Glass (CEGLASS), ITMS code is 313011R453, operational program Research and innovation, co-funded from European Regional Development Fund.

References

- Černošek Z, Holubová J. The structure and certain properties of $\text{CaO-In}_2\text{O}_3\text{-P}_2\text{O}_5$ glasses. *J Non-Cryst Solids*. 2018;490:44–9.
- Brow RK. Review: the structure of simple phosphate glasses. *J Non-Cryst Solids*. 2000;263–264:1–28.
- Hoppe U. A structural model for phosphate glasses. *J Non-Cryst Solids*. 1996;195:138–47.
- Ray NH. Composition–property relationship in inorganic oxide glasses. *J Non-Cryst Solids*. 1974;15:1423–34.
- Brow RK, Alam TM, Tallant DR, Kirkpatrick RJ. Spectroscopic studies of phosphate sealing glasses. *MRS Bull*. 1998;23:63–7.
- Sales C, Boatner LA. Lead-iron phosphate glass: a stable storage medium for highlevel nuclear waste. *Science*. 1984;226:45–8.
- Neel EAA, Pickup DM, Valappil SP, Newport RJ, Knowles JC. Bioactive functional materials: a perspective on phosphate-based glasses. *J Mater Chem*. 2009;19:690–701.
- Buriti S, Barreto J, Barbosa MEV, Barbosa FC, et al. Synthesis and characterization of Ag-doped 45S5 bioglass and chitosan/45S5-Ag

- biocomposites for biomedical applications. *J Therm Anal Calorim*. 2020. <https://doi.org/10.1007/s10973-020-09734-4>.
- Goj P, Ciecińska M, Szumera M, Stoch P. Thermal properties of $\text{Na}_2\text{O-P}_2\text{O}_5\text{-Fe}_2\text{O}_3$ polyphosphate glasses. *J Therm Anal Calorim*. 2020. <https://doi.org/10.1007/s10973-020-09476-3>.
- Ciecińska M, Goj P, Stoch A, Stoch P. Thermal properties of $60\text{P}_2\text{O}_5\text{-(40-x)Al}_2\text{O}_3\text{-xNa}_2\text{O}$ glasses. *J Therm Anal Calorim*. 2019. <https://doi.org/10.1007/s10973-019-08606-w>.
- Zemenová P, Král R, Rodová M, Nitsch K, Nikl M. Calculations of Avrami exponent and applicability of Johnson–Mehl–Avrami model on crystallization in $\text{Er:LiY(PO}_3)_4$ phosphate glass. *J Therm Anal Calorim*. 2019. <https://doi.org/10.1007/s10973-019-09068-w>.
- Vedishcheva NM, Wright AC. Chemical structure of oxide glasses: a concept for establishing structure–property relationships. In: Schmelzer JWP, editor. *GLASS Selected properties and crystallization*, 9. De Gruyter: Berlin; 2014. p. 269–89 (ISBN 978-3-11-029838-3).
- Vedishcheva NM, Shakhmatkin BA, Shultz MM, Wright AC. The thermodynamic modelling of glass properties: a practical proposition? *J Non-Cryst Solids*. 1996;196:239–43.
- Shakhmatkin BA, Vedishcheva NM, Wright AC. Can thermodynamics relate the properties of melts and glasses to their structure? *J Non-Cryst Solids*. 2001;293–295:220–36.
- Vedishcheva NM, Shakhmatkin BA, Wright CA. Thermodynamic modeling of the structure of glasses and melts: single-component, binary and ternary systems. *J Non-Cryst Solids*. 2001;293–295:312–7.
- Vedishcheva NM, Shakhmatkin BA, Wright CA. The structure of sodium borosilicate glasses: thermodynamic modeling vs. experiment. *J Non-Cryst Solids*. 2004;345–346:39–44.
- Macháček J, Chromčíková M, Liška M. Parameterization and validation of thermochemical models of glass by advanced statistical analysis of spectral data. In: Šesták J, Hubík P, Mareš J, editors. *Thermal physics and thermal analysis: from macro to micro, highlighting thermodynamics kinetics and nanomaterials*. Cham: Springer; 2017. p. 257–78 (ISBN 978-3-319-45897-7).
- Liška M, Chromčíková M. Thermal properties and related structural and thermodynamic studies of oxide glasses. In: Šesták J, Holeček M, Málek J, editors. *Glassy, amorphous and nano-crystalline materials: thermal physics, analysis, structure and properties*. Springer: New York; 2011. p. 179–97 (ISBN 978-90-481-2882-2).
- Chromčíková M, Liška M, Karell R, Gašpáreková E, Vlčková P. Thermodynamic model and physical properties of selected zirconia containing silicate glasses. *J Therm Anal Calorim*. 2012;109:831–40.
- Chromčíková M, Liška M, Macháček J, Šulcová J. Thermodynamic model and structure of $\text{CaO-P}_2\text{O}_5$ glasses. *J Therm Anal Calorim*. 2013;114:785–9.
- Kalenda P, Koudelka L, Mošner P, Beneš L, Drobná H. Thermoanalytical study and crystallization of $\text{Ba(PO}_3)_2\text{-WO}_3$ glasses. *J Therm Anal Calorim*. 2019. <https://doi.org/10.1007/s10973-019-08115-w>.
- Chromčíková M, Liška M, Zemanová V, Pliško A, Hruška B, Gavenda T. Thermodynamic model and Raman spectra of $\text{CaO-P}_2\text{O}_5$ glasses. *J Therm Anal Calorim*. 2015;121:269–74.
- Liška M, Lissová M, Pliško A, Chromčíková M, Gavenda T, Macháček J. Thermodynamic model and Raman spectra of $\text{ZnO-P}_2\text{O}_5$ glasses. *J Therm Anal Calorim*. 2015;121:85–91.
- Hruška B, Osipov AA, Osipova LM, Chromčíková M, Černá A, Liška M. Thermodynamic model and high-temperature Raman spectra of $25\text{Na}_2\text{O.75B}_2\text{O}_3$ glassforming melts. *J Therm Anal Calorim*. 2018;133:429–33.
- Voňka P, Leitner J. Calculation of chemical equilibria in heterogeneous multicomponent systems. *Calphad*. 1995;19:25–36.
- Bale WCh. Facility for the analysis of chemical thermodynamics. 2019. <http://www.crct.polymtl.ca/facit/>. Accessed 17 April 2017.
- Bale CW, Bétille E, Chartrand P, Decterov SA, Eriksson G, Hack K, Jung IH, Kang YB, Melançon J, Pelton AD, Robelin C, Petersen S.

- FactSage thermochemical software and databases—recent developments. *Calphad*. 2009;33:295–311.
28. Malfait WJ, Zakaznova-Herzog VP, Halter WE. Quantitative Raman spectroscopy: high-temperature speciation of potassium silicate melts. *J Non-Cryst Solids*. 2007;353:4029–42.
 29. Malfait WJ, Halter WE. Structural relaxation in silicate glasses and melts: results from high-temperature Raman spectroscopy. *Phys Rev B*. 2008;77:014201.
 30. Malfait WJ. Quantitative Raman spectroscopy: speciation of cesium silicate glasses. *J Raman Spectrosc*. 2009;40:1895–901.
 31. Malinowski ER. *Factor analysis in chemistry*. 3rd ed. New York: Wiley; 2002.
 32. Applied Chemometrics. *Factor analysis toolbox for MATLAB®*. 2018. <http://www.chemometrics.com>. Accessed 18 April 2017.
 33. Castro SAD, Virgens CF. Thermal decomposition of *Nephelium lappaceum* L. peel. *J Therm Anal Calorim*. 2019;137:1–9.
 34. Ruckebusch C, Blanchet L. Multivariate curve resolution: a review of advanced and tailored applications and challenges. *Anal Chim Acta*. 2013;765:28–36.
 35. Eigenvector Research. 2020. http://www.eigenvector.com/courses/EigenU_MCR.html. Accessed 15 July 2019.
 36. Daniel JSP, Cruz JC, Catelani TA, et al. Erythromycin-excipients compatibility studies using the thermal analysis and dynamic thermal infrared spectroscopy coupled with chemometrics. *J Therm Anal Calorim*. 2020. <https://doi.org/10.1007/s10973-020-09691-y>.
 37. Mošner P, Račický A, Koudelka L. Thermal properties and crystallization of MgO–FeOx–P₂O₅ glasses. *J Therm Anal Calorim*. 2018;132:843–50. <https://doi.org/10.1007/s10973-018-6981-9>.
 38. Osipov AA, Osipova LM. Structural studies of Na₂O–B₂O₃ glasses and melts using high-temperature Raman spectroscopy. *Phys B*. 2010;405:4718–32.

Publisher's Note Springer Nature remains neutral with regard to jurisdictional claims in published maps and institutional affiliations.